Anomalous density, sound velocity, and structure of pressure-induced amorphous quartz

Sylvain Petitgirard,[1,2,*] Christoph J. Sahle,[3,†] Wim J. Malfait,[4] Georg Spiekermann,[2] Ingrid Blanchard,[1] Eleanor S. Jennings,[1] Marine Cotte,[3,5] and Motohiko Murakami[2]

[1]*Bayerisches Geoinstitut, University of Bayreuth, Bayreuth, D-95440, Germany*

[2]*Department of Earth Sciences, ETH Zürich, Zürich 8025, Switzerland*

[3]*ESRF, The European Synchrotron, 71 Avenue des Martyrs, CS40220, 38043 Grenoble Cedex 9, France*

[4]*Building Energy Materials and Components, Swiss Federal Laboratories for Materials Science and Technology, Empa, 8600 Dübendorf, Switzerland*

[5]*Sorbonne Universités, UPMC Univ Paris 06, CNRS, UMR 8220, Laboratoire d'archéologie moléculaire et structurale (LAMS), 4 Place Jussieu 75005 Paris, France*

(Received 15 October 2021; revised 30 December 2021; accepted 3 March 2022; published 14 April 2022)

The study of quartz and other silica systems under pressure is one of the most prolific domains of research over the past 50 years because of their applications in material science and fundamental relevance to planetary interiors. The characterization of the amorphous state is essential for the comprehension of pressure-induced amorphization of minerals, the metamorphism observed in shocked materials, and the study of melt structures under pressure. Here, we measured *in situ*, under static compression the density, sound velocities, and electronic structure of quartz as it passes through its pressure-induced amorphization transition. The transition pressure could be derived from the abrupt increase in density and sound velocity at 24 GPa, and from strong changes in the silicon $L_{2,3}$ edge and oxygen K edge between 22 and 27 GPa observed in x-ray Raman scattering data, confirming previous results from x-ray diffraction. Above this pressure, our data show an anomalous behavior in density, sound velocity, and electronic fine structure compared to the cold compressed glass and other silica polymorphs. The pressure-induced amorphous quartz has a lower density relative to that of the compressed glass, consistent with the lower average coordination inferred from a different signature in the Si $L_{2,3}$ and O K electronic absorption edges measured by x-ray Raman scattering spectroscopy. This behavior sheds light on the pressure limit of tetrahedral units in SiO_2 components and the existence of polyamorphism in network-forming materials, and highlights the possibility to discriminate between different amorphous states with x-ray Raman scattering spectroscopy.

DOI: 10.1103/PhysRevB.105.134106

I. INTRODUCTION

High-pressure mineral phases naturally occur in ejecta from terrestrial impact craters or in shocked meteoritic materials, and are assumed to be produced during the shock-induced, high-pressure high-temperature conditions during the collision. The determination of the phase assemblage may be used to deduce the p-T conditions at their origin, which in turn constrain the size and velocity of the impactor [1]. In such materials, amorphous silicate phases have been reported to be common, and they are often mixed and in contact with high-pressure crystal phases of the same composition, for instance the presence of SiO_2 diaplectic glass with coesite and stishovite [2,3]. Recovered samples from shock experiments also consist mostly of amorphous material, with trace quantities of stishovite [4]. However, in all recovered samples (natural and experimental), it remains unclear whether the glass originates from the quenched high-temperature melt or it is the product of pressure-induced amorphization.

Numerous shock experiments have been carried out on silicates to reproduce possible conditions of natural meteorite impacts [5–7] or to study planetary interior conditions [8–10]. Products recovered from these experiments have shown the formation of glasses with feldspathic or silicic composition, which are also commonly found at impact sites. High-density glasses with plagioclase composition, maskelynites, have been observed in natural material [11–13] and have also been produced at high pressure without fusion [14]. For compressed quartz, most experimental works, under static as well as dynamic compression, have characterized transition pressures, melting temperature, or velocities [15–17], but these experiments were limited to *in situ* observations about the physical properties and structural evolution during the amorphization process and not of the amorphous phase itself, mostly due to technical challenges. To our knowledge there are no data about the structure and properties of the amorphous phase created during cold compression regime. As an additional complication, the behavior of quartz under dynamic compression differs from the one under static compression. Under shock compression of quartz, a mixed-phase region occurs between 15 and 35 GPa, prior to a transformation into a monoclinic high-pressure phase, which has long been assumed to be stishovite [15,18]. However, a recent report

*Corresponding author: Sylvain.Petitgirard@erdw.ethz.ch
†Corresponding author: Christoph.Sahle@esrf.fr

on shock-compressed α-quartz identified a mixture of weakly scattering crystalline phases between 20 and 35 GPa before converting to a niccolite (hexagonal, d-NiAs) phase above 35 GPa with a lower density than stishovite and possibly combined with a dense amorphous phase [19]. A similar niccolite phase was also previously reported from diamond-anvil cell (DAC) experiments at moderate temperature and pressure [20], which is also associated with an amorphous phase. The degree, or amount, of amorphization inversely correlates with the hydrostaticity of the experiment: the less hydrostatic, the greater the amorphization. The proportion of amorphous versus crystalline phase is difficult to evaluate although it seems that under static compression above 30 GPa most of the sample has amorphized [20]. It is important to note that the thermodynamic paths followed during shock-wave experiments and static experiments are very different: the generation of high temperature along the Hugoniot may lead to the formation of transient species during dynamic compression that may not be observed in recovered samples or *in situ* under static compression. Further, the kinetics in dynamic experiments may not fully reproduce the conditions at impact sites potentially precluding a complete reconstructive transformation from α-quartz to stishovite [21]. From our knowledge, there are no structural details about the amorphous phases recovered from shock or cold-compressed experiments nor from meteoritic or impacted material, and there are no methods to discriminate different signatures between such amorphous phases at present.

Earlier works on α-quartz under quasihydrostatic conditions have reported new crystalline structures for GeO_2 quartz [22] and SiO_2 quartz [23,24], but with a poor crystallinity combined with a strong amorphous signal. These studies proposed that an intermediate structure, quartz II, appears prior to the amorphization between 21 and 30 GPa. Such high-pressure metastable forms of oxides exhibit a lower density than the stable polymorph in the high-pressure regime: the rutile structure, called stishovite for SiO_2. Studies that have used a highly hydrostatic environment, like helium, reported the transformation of α-quartz into the successive form of quartz II between 21 and 30 GPa and beyond to a monoclinic $P2_1/c$ phase, recoverable at ambient conditions [24]. There are, however, no data about this phase *in situ* at high pressure under nonhydrostatic conditions because it has an insufficient crystallinity for proper structural refinement. Overall, the properties of the mixed amorphous and crystalline phases remain unknown. Similar phenomena were also reported for cristobalite under hydrostatic compression, with a variety of metastable crystal structures with mixed Si coordination numbers from 4, 5 to 6 [25,26]. All these intermediate phases display a lower density and incomplete conversion to a hexagonally closest-packed oxygen lattice like stishovite.

For static high-pressure experiments under nonhydrostatic conditions, the structure or physical properties of the pressure-induced amorphized phases remain poorly known and poorly characterized *in situ*. In most cases, the analysis is based on the recovered samples using optical Raman spectroscopy and electron microscopy imaging [17]. Pressure-induced amorphization under static and nonhydrostatic conditions is a well-known phenomenon and has been reported for a large variety of framework structures like H_2O ice [27], the latter being dependent on the kinetic conditions [28], SiO_2 and other silicates like feldspar [29,30]. Experimental *in situ* data on density and the electronic fine structure of such pressure-induced amorphous phases could shed new light on their behavior and might be applied to study amorphous materials recovered from shock experiment or impact sites and this approach has not been tested yet. So far, there has not been any *in situ* evidence of difference in properties or structure between a pressure-induced amorphous phase and its glassy counterpart under pressure. There is also a lack of structural information to compare amorphous systems with crystal structures under pressure because conventional techniques like total x-ray scattering (x-ray diffraction) cannot provide the same level of information when applied to the amorphous phases. Although it is suspected that the structure of amorphized-quartz and SiO_2 glass may be different based on Raman observations of recovered high-pressure run products [17], there is no direct *in situ* information of the structure nor any information about the density relative to the crystalline mineral counterpart, or glass, beyond the pressure-induced amorphous transition. This is mainly due to the difficulty in characterizing such material, combined with the common use of nonspecific probes that do not access the local environment of element but rather probe medium-range structures.

On the other hand, there has been considerable work to study cold compressed glass with particular emphasis on the change of structure and coordination number with pressure. The transformations and behavior of silicate glasses at high pressure have raised considerable attention because they can be used to mimic and interpret the fate of melts in the deep Earth [31–35]. Such questions have been addressed mainly using total x-ray scattering [32,33,36], and optical probes such as Raman [30,37] or Brillouin [38,39] spectroscopy. However, these techniques give information on the intermediate range structure or on the bulk property of the material and are not element specific. Thus, data on the local electronic environment and structure of the main constituent of silicates (Si, O, Mg, Al, etc.) can bring new information on the behavior of glasses and the induced amorphization of silicate minerals at high pressure. Element-specific data combined with bulk properties (i.e., density, velocity) of pressure-induced amorphization can thus reveal the variety of amorphous phases and thermodynamic paths during shock and static compression but also on recovered samples from experiments, found in ejecta in impact sites or in shocked meteorites.

Until recently, the Si and O local electronic structure, reflecting the local coordination, has remained inaccessible at high pressure because the signal of soft x-ray absorption spectroscopy or electron energy-loss spectroscopy is fully attenuated in the first micrometers of the anvils or gaskets in DACs. Recent advances in inelastic x-ray scattering, like x-ray Raman scattering (XRS) spectroscopy methods can however circumvent such issues [40,41]. One of the great potentials of high-pressure XRS is the ability to probe the local electronic environment of low-Z elements even in disordered material, as well as confined in a large sample environment, providing essential data on the structure and properties of amorphous compounds under high-pressure conditions [42].

Here, we report the density and sound velocities of pressure-induced amorphous SiO_2 quartz as determined by

x-ray attenuation measurements and Brillouin scattering, respectively, and investigate the structure of the electronic orbitals involved in the bonding between silicon and oxygen, namely Si $L_{2,3}$ edge and O K edge using XRS spectroscopy. The data point to an anomalous density and velocity behavior in the pressure-induced amorphous phase compared to the cold compressed glass that can be linked to a different electronic structure. The ability of XRS measurements to identify a different signature in the amorphized quartz compared to the glass highlights the potential of the method to discriminate between different amorphous phases of the same chemistry.

II. MATERIALS AND METHODS

A. Materials

A high-purity synthetic quartz crystal was used as starting material and was either double polished down into an ~12-μm thickness plate for the density measurements for the low-pressure run, or ground into a fine powder for high-pressure density measurements and all XRS and Brillouin scattering measurements.

B. Density measurements

The density of quartz through its crystalline-to-amorphous transitions around 23 ± 2 GPa was derived from x-ray attenuation measurements conducted at the ID21 beamline European Synchrotron Radiation Facility (ESRF) (Grenoble, France), at the former side-branch end station [43]. The x-ray beam energy was set at 8.5 keV using a double Si (111) channel-cut monochromator and focused down to $0.7 \times 1\,\mu m^2$ with Kirkpatrick-Baez mirrors. Samples were loaded in beryllium gaskets in BX90 diamond-anvil cells equipped with diamond anvils with 350- or 250-μm culets for low-pressure (0–22 GPa) and high-pressure runs (0-47 GPa), respectively. For the low-pressure run, quartz pieces with sharp edges from the double-polished plate were selected and immersed in methanol:ethanol (4:1) together with a ruby sphere in order to follow the ruby R1 luminescence line shift [44] to determine the pressure. For the high-pressure run, the sample chamber in the Be gasket was filled with powder sample and the pressure was determined using the Raman T_{2g} mode of the diamond anvil [45]. The uncertainty in pressure is estimated to be between 0.1 and 0.2 GPa for the low-pressure run (ruby luminescence) and 0.2 to 0.4 GPa for the high-pressure run (Raman of diamond anvil). On the beamline, the measurement strategy was similar to that employed previously for $MgSiO_3$, SiO_2, and GeO_2 glasses [35,46,47], using 2D x-ray absorption mapping of the sample under two orientations: (i) through the diamond, with a Y-Z map, to extract the lateral extension of the sample and obtain the path length (x) of the x rays through the sample during the measurements through the gasket [Figs. 1(a) and 1(b)], and (ii) through the Be gasket, with an X-Z map, in order to measure the x-ray attenuation (I/I_0) of the sample under pressure [Figs. 1(c) and (1d)]. The edges of the sample, defining the path length (x), can be obtained with a precision better than 2 μm, corresponding to uncertainty of about 2% on the density. The uncertainties associated with the absorption are linked to the electronic of the counting device (e.g., Si diode or ionization chamber) and the fluctuation are usually less than 0.2%. The absorbance (μ_{HP}) of the sample was extracted from the correlation between the x-ray attenuation and the path length of the sample obtained from both maps [Fig. 1(e)]. Further details of the method and its associated uncertainties can be found elsewhere [48]. The slope of the linear regression gives the linear absorbance at high pressure (μ_{HP}) via the Beer-Lambert relation:

$$\ln(I/I_0) = -\mu_{HP} x. \tag{1}$$

The density at high pressure (ρ_{HP}) was then calculated by

$$\rho_{HP}/\mu_{HP} = \rho_0/\mu_0. \tag{2}$$

The attenuation coefficient at ambient pressure (μ_0) was determined from the absorption of a thicker double-polished plate from the same quartz sample using the same setup on the beamline, and we used literature data for the ambient pressure density (ρ_0) at $2.652 \pm 0.008\,g/cm^3$ [49].

C. Brillouin and optical Raman spectroscopy

We conducted Brillouin and optical Raman spectroscopy in-house at ETH Zūrich. The Brillouin scattering measurements were carried out at room temperature in a BX90 diamond-anvil cell [50]. The powder quartz sample was loaded into a 100-μm-diameter hole in a rhenium gasket without a pressure-transmitting-medium and compressed between 250-μm culet diamonds. Pressure was determined using the Raman T_{2g} mode of the diamond-anvil tip [45]. An Ar laser with a wavelength of 532 nm was used as the probe beam focused to a spot size of about 10 μm. The scattered light was analyzed through a Sandercock-type 6-pass tandem Fabry-Perot interferometer as described elsewhere [51]. The collection geometry for the Brillouin experiments was set at a scattering angle of 50° and carefully measured using a standard reference BK7 glass with known sound-wave velocities at ambient conditions [52]. The collecting time for a single Brillouin scattering measurement was between 6 and 12 h. At each pressure, the raw Brillouin spectra of Stokes and anti-Stokes peaks were fitted with Lorentzian functions to obtain the peak positions corresponding to the frequency shift ($\Delta\omega$) and then converted into velocities (V) using the following relationship [53]:

$$V = \frac{\Delta\omega\lambda}{2\sin\left(\frac{\theta}{2}\right)}, \tag{3}$$

where λ is the wavelength of the probe laser, $\Delta\omega$ the frequency shift as measured by the Fabry-Perot interferometer, and θ is the scattering-angle geometry.

After each Brillouin measurement, we collected Raman spectra of the pressurized quartz using a 2500SPi spectrometer, with a 500-cm focal length and a 1800 gr/mm grating combined with a 532-nm laser. The spectra were collected in the 100- to 1200-cm^{-1} range between the Rayleigh line and the diamond peak with a typical collection time of 180 s.

D. XRS spectroscopy

In combination with the density, velocity, and optical Raman data, we characterized the evolution of the electronic

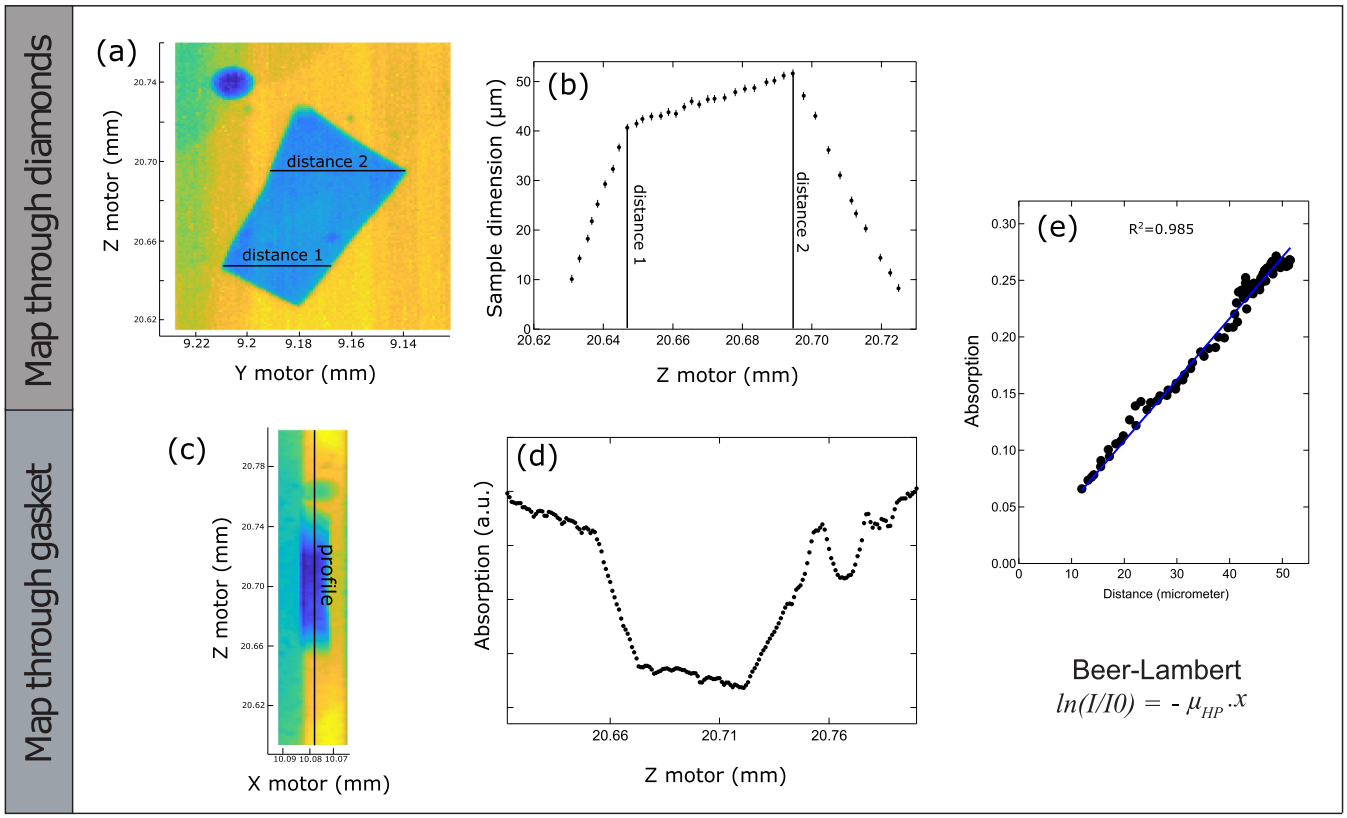

FIG. 1. Density measurement using the x-ray absorption method at ID21, ESRF on the sample at 31.4GPa. A *Y*-*Z* map of the sample is collected through the diamond (a) and allows to extract the dimension of the sample along the *Y* motor axis, as a function of the *Z* motor axis (b). After a 90° rotation, a second *X*-*Z* map is collected through the transparent Be gasket (c) to extract the absorption profile of the sample (d). The combination of path length (c) and absorption (d) permits to retrieve the linear absorbance (μ_{HP}) of the sample (e), thus its density under pressure using Eq. (2).

structure between silicon and oxygen atoms by measuring the fine structure of absorption edges of electrons directly involved in the bonding, namely the Si $L_{2,3}$ edge and the O *K* edge, using XRS spectroscopy performed on the ID20 beamline of the ESRF (Grenoble, France) [54]. The spectrometer elastic line energy was set between 9.8 and 9.83 keV for the Si *L* edge and 10.2 to 10.26 KeV for O *K* edge through a first high heat-load liquid-nitrogen cooled Si(111) premonochromator and a final incident bandwidth of approximately 0.4 eV was obtained using a Si(311) channel-cut post-monochromator. The beam was focused down to $\sim 10 \times 20\,\mu\mathrm{m}^2$ ($V \times H$) through a pair of Kirkpatrick-Baez mirrors. Three out of six spectrometers were used to collect the scattering signal, allowing to probe the sample at different transferred momenta $|q|$ up to a maximum of $10\,\text{Å}^{-1}$. Each spectrometer contains 12 Si(660) spherically curved crystal analyzers that act as focusing monochromators enabling a sub-eV (0.7-eV) final resolution when working in the vicinity of 9.7 keV. The quartz sample was ground into a fine powder and loaded in either PanoDAC or MBX110 diamond-anvil cells from the ESRF sample environment pool [55]. We performed measurements through Be gaskets, with cBN inserts following the procedure described in Ref. [41] using standard conical diamonds with 500-μm culet size at low pressure and 250-μm culet size for higher pressure. All data were treated using the XRStools program package [56].

III. RESULTS

A. Density of pressure-induced amorphous quartz

The density results as a function of pressure are reported in Fig. 2 and Table I. Up to 20 GPa, the increase in density is in fairly good agreement with data obtained from single-crystal x-ray diffraction (XRD) data [57] for both the measurements with and without the methanol-ethanol pressure medium. Below 20 GPa, the quartz follows a compression trend that is well described by a third- (or fourth-)order Birch-Murnaghan equation of state (EoS)with comparable values to the one for single crystal in a hydrostatic medium using XRD [57] (Table II), albeit with larger uncertainties, as expected. In contrast, the glass has a much lower initial density than quartz (2.2 versus $2.65\,\mathrm{g/cm}^3$), but a much higher compressibility [46], and both density trends cross over at about 15–20 GPa. Above 20 GPa, the compressed glass continues on a steep compression path that saturates at about 50 GPa with a clear inflection in the density curve [46] asymptotic to the crystal polymorph densities (Stishovite and $CaCl_2$) [58]. In contrast to this continuous, steep increase in density for the compressed glass, the density of the amorphous quartz displays an abrupt change in density of about 11% at the transition pressure of 23 ± 2 GPa. The amorphized-quartz compression curve follows a less steep increase in density than the compressed

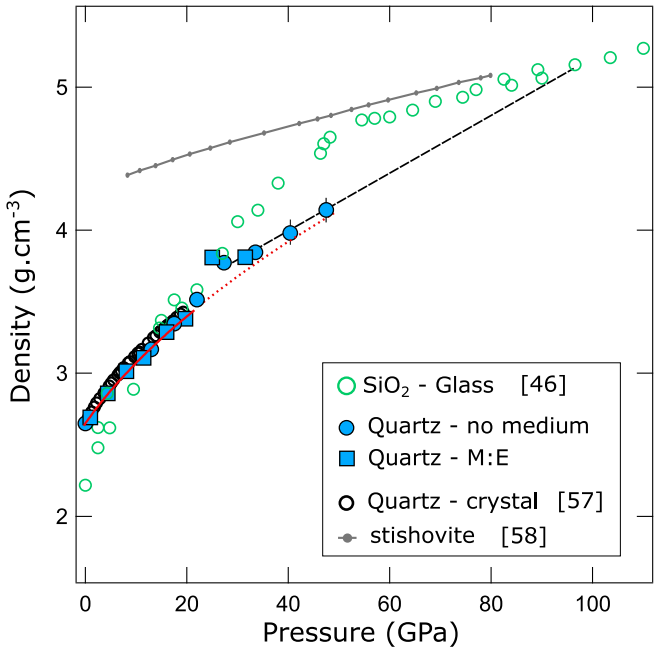

FIG. 2. Density results for the cold compressed quartz, compared to other SiO_2 polymorphs: glass [46] (open green circle, x-ray attenuation), quartz in helium [57] (open black circles, x-ray single-crystal diffraction), and stishovite [58] (gray point and line, XRD powder). The red line corresponds to the Birch-Murnaghan fit and its extrapolation to higher pressure along the dotted red line. The black dashed line corresponds to the linear extrapolation of the density data after the amorphization transition. The errors on pressure are of the size of the symbols. The errors for the density are either reported or are of the size of the symbols.

glass, along an almost linear trend that falls between the extrapolated EoS of quartz and the density of the compressed glass. The linear extrapolation of this trend to higher pressures suggests that the density of pressure-amorphized quartz

TABLE I. Extracted densities for the different pressures including error estimates.

Pressure (GPa)	Error	Density (g cm^{-1})	Error
0	0	2.652	0.008
1.05	0.1	2.696	0.054
4.2	0.2	2.861	0.057
7.9	0.3	3.009	0.060
11.5	0.5	3.113	0.062
12.7	0.5	3.165	0.063
16.2	0.5	3.287	0.099
17.5	0.5	3.348	0.100
19.7	0.7	3.383	0.101
21.9	0.7	3.513	0.105
25.1	0.7	3.809	0.114
26.9	1	3.783	0.113
31.4	1	3.809	0.114
33.4	1	3.852	0.116
40.2	1	3.983	0.119
47.3	1	4.148	0.124

TABLE II. Comparison of EoS parameters between single-crystal x-ray diffraction [57] and absorption from this study. $V0$ in the present work was set to a fixed value.

BM3	V_0	KT_0	K'	
Scheidl *et al.*	112.967	40.1	4.8	
This study	112.967	51.87 (5)	3.54 (0.8)	
BM4	V_0	KT_0	K'	K''
Scheidl *et al.*	112.968	37	6.7	−0.735
This study	112.967	45 (6)	6.78 (1.0)	−0.88

reaches the density of its pressurized glassy counterpart only at about 70 to 80 GPa, i.e., beyond the inflection in the glass density data near 50–60 GPa, which is assumed to be the transformation to almost sixfold in glass [40,46].

The pressure of transition from crystalline to amorphous can be derived from the marked change in density between 22.5 and 25.3 GPa in both types of experiment, with and without the pressure medium, in excellent agreement with previous XRD data [30] and calculations [59]. Across the transition, the density increases by about 11%, somewhat less than the calculated value of 16% [59]. Nevertheless, these two values are quite close and these experimental *in-situ* density data for high-pressure amorphized quartz validate the calculations.

B. Sound velocities of pressure-induced amorphous quartz

The densification at the transition is corroborated by a sharp change in velocities measured by Brillouin spectroscopy, with a sharp increase of the transverse acoustic (TA or Vs) mode. The longitudinal acoustic (LA) mode is masked partially by the TA from the diamond anvil. The Brillouin data display a slow increase in Vs between 0 and 23 GPa, followed by a rapid 20% increase at the transition. This rapid increases in Vs is consistent with the sudden density increase measured at the transition. Above the transition, Vs becomes higher in the pressure-induced amorphized quartz compared to the compressed glass, which may be related to the lower density of the amorphized quartz compared to the glass, but this should be taken with care as Vs also depends on the shear moduli of the material. After this rapid increase, the velocities increase at a much lower rate above 35 GPa, but remain higher than those of compressed silica glass [34] over the investigated pressure range [Fig. 3(d)]. A linear extrapolation to higher pressure indicates that velocities for both the glass and pressure-induced amorphous quartz may reach similar values at about 70–80 GPa, i.e., the same pressure range found when extrapolating the two density trends (see above).

C. Structure of pressure-induced amorphous quartz

From optical Raman measurements we notice that the crystallinity decreases gradually upon compression. At the transition there is a sudden decrease in intensity of the peaks characteristic for the crystalline part; however, these peaks remain observable up to about 35 GPa. This observation in combination with the observed density jump is in good

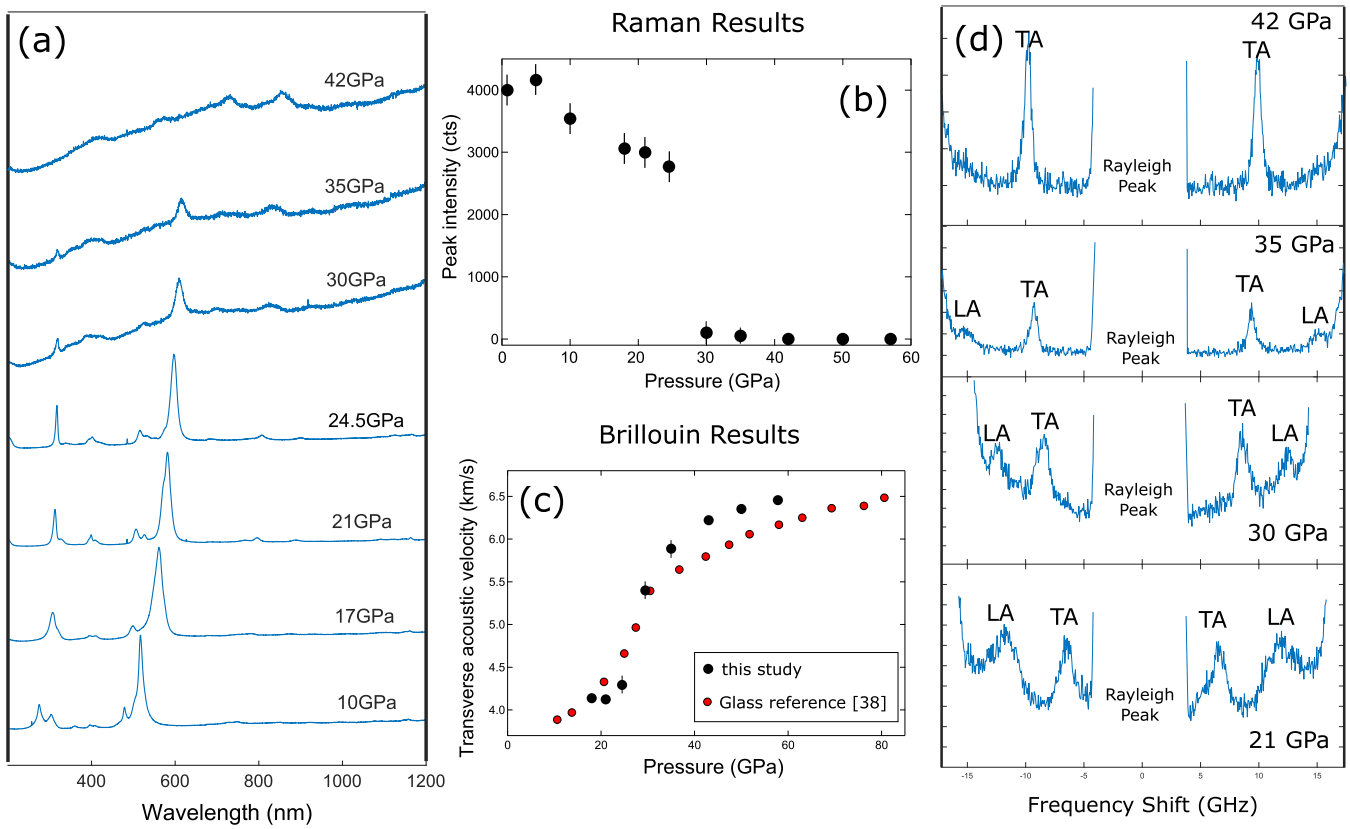

FIG. 3. Optical Raman data and Brillouin spectra on cold compressed quartz. (a) Optical Raman spectra from 10 to 42 GPa. A partial amorphization is observed above 24 GPa and complete loss of crystallinity above 35 GPa. (b) Plot of the main peak (550–600 cm^{-1}) intensity as a function of pressure. From 10 to 24 GPa the peak intensity decreases slowly and sharply drops above this pressure and completely disappears above 35 GPa. (c) Selected Brillouin data at different pressure across the amorphization pressure. The LA peaks disappear above 35 GPa while the TA peaks become sharper with pressure. (d) Transverse velocity as a function of pressure for quartz and compared to the glass data [38]. The trend is relatively linear at low pressure; it shows a sharp increase between 25 and 35 GPa and flattens above 35 GPa, with higher velocities than in the glass.

agreement with earlier studies showing a first-order phase transformation of α-quartz to a superlattice structure at the origin of the transition [59]. The remaining crystalline signatures vanish completely at pressure higher than 35 GPa and suggest that the sample is completely amorphous beyond such pressure, while a crystalline part remains observable between 25 and 35 GPa. This confirms previous observation of the preservation of lamellae of the original fourfold-coordinated structure on recovered sample up to about 30 GPa, but not beyond such pressure [17]. Such a possible persistence of small crystalline characteristics from the original structure is also visible in the Brilllouin spectrum with the decrease and gradual disappearance of the LA velocities still measurable up to 35 GPa [Fig. 3(c)], before it completely disappears beyond this pressure. The TA peaks become very sharp for pressures higher than 35 GPa, as observed for any other glass measured in the same conditions [34], indicating that the stress in the sample has homogenized and the bulk structure has become glasslike, although a small fraction may still persist as crystalline depending on stress conditions [20].

To go beyond optical measurements, the XRS data on the Si $L_{2,3}$ edge and O K edge are of prime importance as they allow probing the electronic environment between the silicon and oxygen atoms. In Fig. 4, we report the absorption edge spectra for both elements as a function of pressure. The Si $L_{2,3}$-edge data show a clear transition at about 24–27 GPa from quartzlike spectra, with an edge onset made of a double feature, to stishovite-like spectra, with a single peak at 108 eV energy loss. The O K edge also shows changes at similar pressures with a spectral shape that evolves towards a stishovite-like spectrum, thus confirming a structural change at this pressure at the origin of the densification measured by the x-ray attenuation technique. To obtain more details about the structural change of the amorphized quartz and to go beyond the qualitative spectral shape, we report in Fig. 5 the evolution of the edge onset as a function of pressure and compare them with edge onsets of other reference materials previously measured [40].

For both the Si $L_{2,3}$ edge and the O K edge, the onset energy values follow a gradual increase at low pressure between 0 and 22 GPa similar to the ones measured on the cold compressed glass, which confirms that the glass and quartz have similar coordination in this pressure range. At the transition pressure ($\sim$24 GPa) the onset values suddenly shift to higher energies as for the glass. For the Si $L_{2,3}$ edge at the transition pressure, the onset energy increases in between the quartz and stishovite

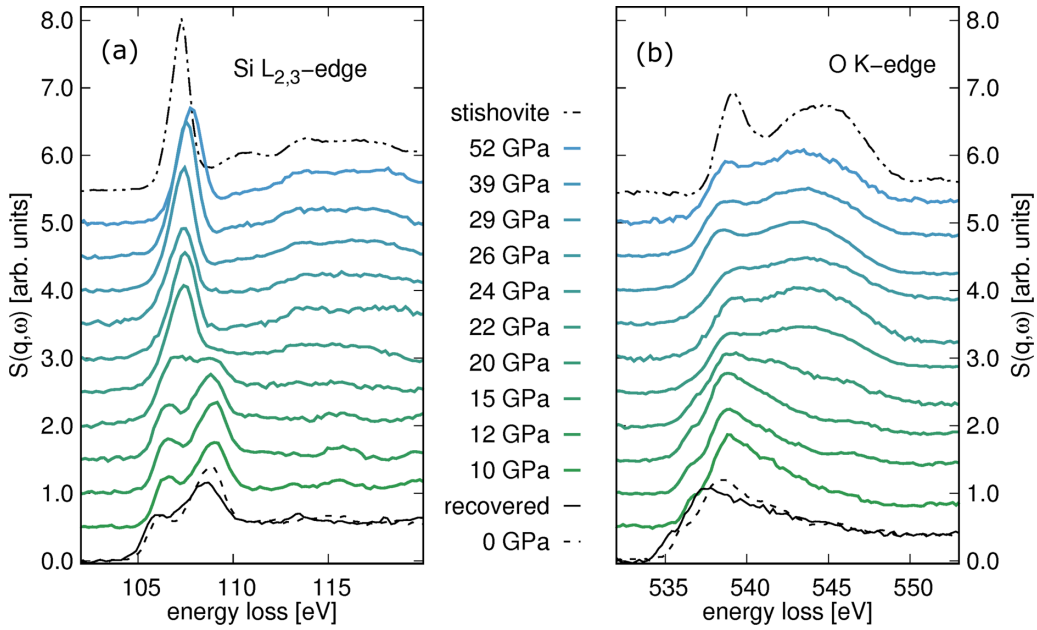

FIG. 4. XRS data on Si and O edges in quartz with pressure collected at ID20. (a) Si $L_{2,3}$ edge as a function of pressure and (b) O K edge with pressure. Both spectra are compared to reference samples at ambient conditions, quartz and stishovite, respectively.

values and continues to evolve linearly upward after that, staying below the glass value in the pressure range covered in this study. For the O K-edge data, the edge onset values closely follow the one measured for the cold compressed stishovite up to 25 GPa. After the transition pressure, the O K-edge data fall below the ones of the cold compressed glass. Above 30 GPa, both edge trends (Si L edge and O K edge) increase linearly with values below the ones measured in the glass. As for the density, when we extrapolate the trend of energy position of the edge onset for amorphous quartz, the data indicate that values for the glass and the pressure-induced amorphous quartz would reach similar values around 70 to 80 GPa. This confirms that the structures continue to evolve with pressure with a gradual change in the coordination or compaction facilitating the densification of both amorphous phases.

IV. DISCUSSION AND CONCLUSION

All reported data converge to similar observations with a preservation of the quartz structure, or fourfold coordination, up to about 22–24 GPa and sudden changes at the transition pressure. Above the transition pressure, the phases created by the amorphization process show distinct characteristics compared to other crystal structures and the cold compressed glass. The density data allow for a direct comparison of a bulk physical property evolution with other silica polymorphs. The pressure-induced amorphized quartz has a lower density than the glass and stishovite at high pressure and may reach similar values only for pressures above 70 GPa. The velocity measurements support the density data and although they remain more qualitative, they still confirm the abrupt change at 25 GPa and also that the velocities in amorphized quartz are different than in the cold compressed glass [38], with higher velocities. Similar to the density, both velocity trends may intersect and reach similar values at about 70–80 GPa. The sharpness of the TA peak after the transition is also a good indicator that the sample is mostly amorphous above 25 GPa and completely amorphous beyond 35 GPa. The latter observation is corroborated by the optical Raman measurements, with traces of crystallinity up to 35 GPa, which may be related to the formation of quartz-II [17,60], and which disappear above this pressure.

From our XRS measurements, we likewise observe strong changes in the spectral shape between ambient and high pressure, with a change from quartz at low pressure to a spectral signature that resembles the stishovite reference sample although with less sharp features at pressure above 25 GPa, especially for the O K edge. A detailed analysis using the edge onset of both edges brings finer clues about the behavior of each silica polymorph under pressure. The edge onset dependence with pressure between 0 and 22 GPa does not show any drastic changes and evolves quite linearly and follows the glass trend measured previously in this pressure range [40]. Beyond 22–25 GPa, we notice that the change in the spectral feature is marked with a clear shift of both edge onsets to higher values.

At the transition pressure, the O K-edge onset sharply evolves to coincide with the values of the stishovite and drops below both the stishovite and the glass at higher pressure ($P > 30$ GPa). At the same time the Si $L_{2,3}$-edge onset evolves more gradually with pressure following the glass trend, but always remaining slightly lower. This suggests that a strong compaction or distortion of the oxygen sublattice takes place but that the coordination of the silicon atoms evolves more gradually from 4 to a higher number (5 and/or 6). The spectroscopic signatures for the O K edge at the transition pressure are comparable to the ones measured for the stishovite reference as well as the glass at such pressure. This clearly indicates the loss of the primary structure to a change of the oxygen sublattice toward a closest-packed structure. For the Si $L_{2,3}$ edge the spectral shape is also similar to both glass

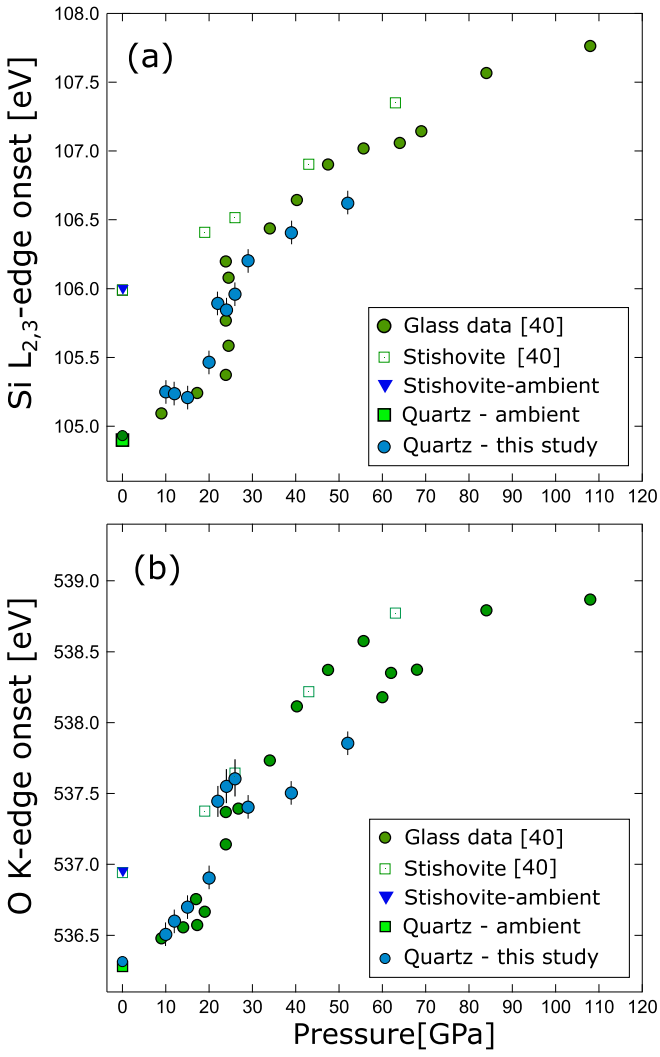

FIG. 5. Si $L_{2,3}$-edge and O K-edge edge onset as a function of P compared to the respective edge onset for the pressurized glass and stishovite reference [40]. (a) Si $L_{2,3}$-edge data for the quartz under nonhydrostatic compression compared to the Si $L_{2,3}$-edge for the glass and stishovite in similar conditions. (b) Results for O K-edge for the quartz, glass, and stishovite.

and stishovite with a single sharp peak. However, a direct comparison is always difficult because the fivefold and sixfold spectra are very similar in shape and are therefore difficult to distinguish [40]. Nevertheless, the presented data hold clear evidence that the fourfold signature has almost completely vanished above 23–25 GPa, giving way to an octahedral oxygen sublattice.

For both the cold compressed glass and pressure-induced amorphized quartz, we notice a clear change in the absorption edges of both Si and O at a pressure around 22–25 GPa. Calculation and data on the Si coordination evolution on glass show a clear drop in fourfold coordination and increase of higher coordination, five and six, at such pressure [61], and we can thus infer a pressure limit for the stability of the native Si-O tetrahedron structure under nonhydrostatic conditions. As shown from the Raman and Brillouin data, weak signs of the initial structure can be preserved slightly beyond this pressure up to 35 GPa. The preservation of fourfold coordination was also reported in SiO_2 crystal polymorphs, like cristobalite, under highly hydrostatic conditions, still with a phase transition in the crystal structure taking place at 22 GPa. Such change in crystal structure goes along with a reduction of the symmetry and a loss of the crystallinity of the sample. Also noticeable, the density trend of the high-pressure cristobalite phases, with mixed coordination silicon above 30 GPa, shows a lower density and compressibility than the sixfold stishovite reference, a feature that we also observe for the high-pressure amorphized quartz.

At higher pressure, previous results both experimental and computational have demonstrated the possibility to obtain a weak crystalline orthorhombic phase at room temperature through the pressure amorphization of quartz via an amorphous state above 60 to 70 GPa [62,63]. Such results implied a decrease of the activation energy for the formation of silica polymorphs with pressure leading to the formation of higher coordination silica, with no insight or physical properties on the intermediate amorphous state. In the present work we show that this mechanism is possible because the tetrahedral network is destabilized at 23 GPa to form a disorganized low-density structure with an increase in Si-O coordination, but still remaining below the glass and stishovite references. It is possible that the pressure-induced amorphous phase is a low-density sixfold silicon, or a mixture of five- and sixfold coordination, with oxygen predominantly forming a closest-packed sublattice. This low-density coordination silicon structure may gradually be rearranged and reordered at higher pressure, or its coordination may continue to evolve, toward sixfold for silicon and reaches stable crystal-like form like stishovite, or $CaCl_2$, with a preferred orientation at about 70–80 GPa, where a low-intensity stihsovite-like structure has been measured elsewhere [62]. It demonstrates that pressure plays a major role in the formation of silica polymorphs even without temperature.

Interestingly, the compressed glass does not show signs of recrystallization at high pressure [32,64] while the amorphized quartz was reported to partially recrystallize into a stishovite-like structure beyond 70 GPa [62]. This seems to suggest that polyamorphism exists for SiO_2 and may also be true for other silicate components or else that pressure-amorphous compounds may not be truly amorphous materials but rather disordered nanostructures that can rearrange and reuse the motif of the primitive structure of the original crystal structure. Such a memory effect, with a loss of crystallinity and reapparition of a weak crystalline signature at higher pressure, could be tested through pressure cycling of the sample from low to high pressure for instance. We can speculate that this memory effect will disappear after a series of pressure cycles and the sample may be completely amorphized at some point.

It is quite possible that such features are common to other systems that undergo pressure-induced amorphization like other silicate minerals or molecular system like water. This clearly illustrates that amorphous material can exhibit a variety of structure and physical parameters with a strong dependence on the initial state and structure of the starting material in order to produce such polyamorphism [65]. Further studies on single-crystal α-quartz compressed under

hydrostatic conditions and analyzed with x-ray diffraction as well as the method presented here (XRS and Brillouin) would bring a clearer view on the structural evolution of the pressure-induced transformation in α-quartz. Further, XRS analysis with a pencil beam of a few microns could be applied to shocked material, either from experiments or from natural impact sites, and may reveal characteristic signatures of the amorphous phases giving information whether they originate from quenched melt, incomplete transformation, or even amorphization after the release of the shock conditions. Our findings demonstrate that, at constant chemical composition, a cold compressed amorphization does not produce a similar amorphous compound compared to a pure cold compressed glass. The choice of the starting material is then of prime importance to study amorphous matter under pressure, for instance starting from nanocrystalline or a crystalline powder, like α-quartz, may not result in the same amorphous material under pressure and essentially not reflect the pure glass of the same composition like for TiO_2 [66]. The combination of methods including element-specific probes, like XRS, are then essential for measuring structural changes in amorphous materials, pressure induced or not, as it allows discriminating between different amorphous states, that can be misleading for the interpretation of structural changes in amorphous matter under pressure. Like for shock experiments, the starting material results in different paths for the amorphous and crystalline phase. The shock compression of α-quartz produces a low-density hexagonal (d-NiAs) phase [19] in contrast to the glass that transforms directly to stishovite [67]. Here we show that the cold compression of α-quartz results in a low-density amorphous phase compared to the cold compressed glass. This result explains the possible mechanisms for such differences reported in shock experiments with a low kinetic barrier to cross for the transformation of the glass to the stishovite, because their density and structure are very close to each other. In the case of α-quartz a much higher kinetic barrier exists to transform it into stishovite and the formation of a d-NiAs structure is favored due to the mild p-T conditions produced during the shock. Similar results have been also achieved in static compression experiment with mild temperature conditions [20]. Significantly higher temperatures may however allow crossing such barriers and directly convert the α-quartz to stishovite. Recovered samples from impact sites or meteorites that have been shocked can thus exhibit a large variety of structures depending on the p-T conditions, and finer analysis of the electronic environment of their major elements (Si, O …) may thus reveal more details about their thermodynamic pathways.

ACKNOWLEDGMENTS

We are particularly grateful to H. Shultz and R. Njul for the polishing of the starting samples prior to the beamtime. We are thankful to M. Hanfland for the access and use of the off-line Raman system of beamline ID15B. D. Bugnazet and M. Salomé are thanked for their help in designing the sample holder for ID21 measurements. We acknowledge the ESRF for provision of beamtime under the Proposals No. ES-354 and No. ES-590. S.P. was financed by DFG Grant No. PE2334/1-1.

[1] P. Beck, P. Gillet, A. El Goresy, and S. Mostefaoui, Timescales of shock processes in chondritic and Martian meteorites, Nature (London) **435**, 1071 (2005).

[2] M. Miyahara, E. Ohtani, A. Yamaguchi, S. Ozawa, T. Sakai, and N. Hirao, Discovery of coesite and stishovite in eucrite, Proc. Natl. Acad. Sci. USA **111**, 10939 (2014).

[3] M. Miyahara, S. Kaneko, E. Ohtani, T. Sakai, T. Nagase, M. Kayama, H. Nishido, and N. Hirao, Discovery of seifertite in a shocked lunar meteorite, Nat. Commun. **4**, 1737 (2013).

[4] V. Staehle, R. Altherr, M. Koch, and L. Nasdala, Shock-induced growth and metastability of stishovite and coesite in lithic clasts from suevite of the Ries Impact Crater (Germany), Contrib. Miner. Petr. **155**, 457 (2008).

[5] E. V Petrova, V. I. Grokhovsky, T. Kohout, R. F. Muftakhetdinova, and G. A. Yakovlev, Shock-wave experiment with the Chelyabinsk LL5 Meteorite: Experimental parameters and the texture of the shock-affected material, Geochem. Int. **57**, 923 (2019).

[6] A. E. Gleason, C. A. Bolme, H. J. Lee, B. Nagler, E. Galtier, D. Milathianaki, J. Hawreliak, R. G. Kraus, J. H. Eggert, D. E. Fratanduono, G. W. Collins, R. Sandberg, W. Yang, and W. L. Mao, Ultrafast visualization of crystallization and grain growth in shock-compressed SiO_2, Nat. Commun. **6**, 8191 (2015).

[7] M. Millot, S. Zhang, D. E. Fratanduono, F. Coppari, S. Hamel, B. Militzer, D. Simonova, S. Shcheka, N. Dubrovinskaia, L. S. Dubrovinsky, and J. H. Eggert, Recreating giants impacts in the laboratory: Shock compression of $MgSiO_3$ Bridgmanite to 14 Mbar, Geophys. Res. Lett. **47**, 1 (2020).

[8] M. Millot, N. Dubrovinskaia, A. Cernok, S. Blaha, L. Dubrovinsky, D. G. Braun, P. M. Celliers, G. W. Collins, J. H. Eggert, and R. Jeanloz, Shock compression of stishovite and melting of silica at planetary interior conditions, Science **347**, 418 (2015).

[9] J. A. Akins, S.-N. Luo, P. D. Asimow, and T. J. Ahrens, Shock-induced melting of $MgSiO_3$ perovskite and implications for melts in Earth's lowermost mantle, Geophys. Res. Lett. **31**, L14612 (2004).

[10] J. L. Mosenfelder, P. D. Asimow, and T. J. Ahrens, Thermodynamic properties of Mg2SiO4 liquid at ultra-high pressures from shock measurements to 200 GPa on Forsterite and Wadsleyite, J. Geophys. Res. Solid Earth **112**, B06208 (2007).

[11] T. E. Bunch, A. J. Cohen, and M. R. Dence, Natural terrestrial Maskelynite, Am. Mineral. **52**, 244 (1967).

[12] R. V Gibbons and T. J. Ahrens, Effects of shock pressures on calcic Plagioclase, Phys. Chem. Miner. **1**, 95 (1977).

[13] M. Kitamura, T. Goto, and Y. Syono, Intergrowth textures of diaplectic glass and crystal in shock-loaded P-Anorthite, Contrib. to Mineral. Petrol. **61**, 299 (1977).

[14] D. J. Milton and P. S. de Carli, Maskelynite: Formation by explosive shock, Science **140**, 670 (1963).

[15] J. A. Akins and T. J. Ahrens, Dynamic compression of SiO_2: A new interpretation, Geophys. Res. Lett. **29**, 31-1 (2002).
[16] R. J. Hemley, H. K. Mao, P. M. Bell, and B. O. Mysen, Raman-spectroscopy of SiO_2 Glass at High Pressure, Phys. Rev. Lett. **57**, 747 (1986).
[17] K. J. Kingma, C. Meade, R. J. Hemley, H. K. Mao, and D. R. Veblen, Microstructural observations of alpha-quartz amorphization, Science **259**, 666 (1993).
[18] R. G. McQueen, J. N. Fritz, and S. P. Marsh, On equation of state of stishovite, J. Geophys. Res. **68**, 2319 (1963).
[19] S. J. Tracy, S. J. Turneaure, and T. S. Duffy, Structural response of alpha-quartz under plate-impact shock compression, Sci. Adv. **6**, eabb3913 (2020).
[20] L. S. Dubrovinsky, N. A. Dubrovinskaia, V. Prakapenka, F. Seifert, F. Langenhorst, V. Dmitriev, H. P. Weber, and T. Le Bihan, A class of new high-pressure silica polymorphs, Phys. Earth Planet. Int. **143**, 231 (2004).
[21] F. Langenhorst and A. Deutsch, Shock metamorphism of minerals, Elements **8**, 31 (2012).
[22] J. Haines, J. M. Leger, and C. Chateau, Transition to a crystalline high-pressure phase in a-GeO_2 at room temperature, Phys. Rev. B **61**, 8701 (2000).
[23] K. J. Kingma, R. J. Hemley, H. K. Mao, and D. R. Veblen, New High-Pressure Transformation in Alpha-Quartz - Reply, Phys. Rev. Lett. **72**, 1302 (1994).
[24] J. Haines, J. M. Leger, F. Gorelli, and M. Hanfland, Crystalline Post-Quartz Phase in Silica at High Pressure, Phys. Rev. Lett. **87**, 155503 (2001).
[25] E. Bykova, M. Bykov, A. Cernok, J. Tidholm, S. I. Simak, O. Hellman, M. P. Belov, I. A. Abrikosov, H.-P. Liermann, M. Hanfland, V. B. Prakapenka, C. Prescher, N. Dubrovinskaia, and L. Dubrovinsky, Metastable silica high pressure polymorphs as structural proxies of deep earth silicate melts, Nat. Commun. **9**, 4789 (2018).
[26] A. Cernok, E. Bykova, T. B. Ballaran, H.-P. Liermann, M. Hanfland, and L. Dubrovinsky, High-pressure crystal chemistry of Coesite-I and its transition to Coesite-II, Z. Krist. Cryst. Mater. **229**, 761 (2014).
[27] C. Lin, X. Yong, J. S. Tse, J. S. Smith, S. V Sinogeikin, C. Kenney-Benson, and G. Shen, Kinetically Controlled Two-Step Amorphization and Amorphous-Amorphous Transition in Ice, Phys. Rev. Lett. **119**, 135701 (2017).
[28] C. A. Tulk, J. J. Molaison, A. R. Makhluf, C. E. Manning, and D. D. Klug, Absence of Amorphous Forms when Ice Is Compressed at Low Temperature, Nature (London) **569**, 542 (2019).
[29] I. Daniel, P. Gillet, P. F. McMillan, G. Wolf, and M. A. Verhelst, High-pressure behavior of anorthite: Compression and amorphization, J. Geophys. Res. Earth **102**, 10313 (1997).
[30] R. J. Hemley, A. P. Jephcoat, H. K. Mao, L. C. Ming, and M. H. Manghnani, Pressure-induced amorphization of crystalline silica, Nature (London) **334**, 52 (1988).
[31] C. Meade and R. Jeanloz, Effect of coordination change on the strength of amorphous SiO_2, Science **241**, 1072 (1988).
[32] T. Sato and N. Funamori, High-pressure structural transformation of SiO_2 glass up to 100 GPa, Phys. Rev. B **82**, 184102 (2010).
[33] C. Sanloup, J. W. Drewitt, Z. Konopkova, P. Dalladay-Simpson, D. M. Morton, N. Rai, W. VanWestrenen, and W. Morgenroth, Structural change in molten basalt at deep mantle conditions, Nature (London) **503**, 104 (2013).
[34] M. Murakami, S. Kohara, N. Kitamura, J. Akola, H. Inoue, A. Hirata, Y. Hiraoka, Y. Onodera, I. Obayashi, J. Kalikka, N. Hirao, T. Musso, A. S. Foster, Y. Idemoto, O. Sakata, and Y. Ohishi, Ultrahigh-pressure form of SiO_2 glass with dense pyrite-type crystalline homology, Phys. Rev. B **99**, 045153 (2019).
[35] S. Petitgirard, W. J. Malfait, R. Sinmyo, I. Kupenko, L. Hennet, D. Harries, T. Dane, M. Burghammer, and D. C. Rubie, Fate of $MgSiO_3$ melts at core-mantle boundary conditions, Proc. Natl. Acad. Sci. USA **112**, 14186 (2015).
[36] C. J. Benmore, E. Soignard, S. A. Amin, M. Guthrie, S. D. Shastri, P. L. Lee, and J. L. Yarger, Structural and topological changes in silica glass at pressure, Phys. Rev. B **81**, 054105 (2010).
[37] S.-H. Shim and K. Catalli, Compositional dependence of structural transition pressures in amorphous phases with mantle-related compositions, Earth Planet. Sci. Lett. **283**, 174 (2009).
[38] M. Murakami and J. D. Bass, Spectroscopic Evidence for Ultrahigh-Pressure Polymorphism in SiO_2 Glass, Phys. Rev. Lett. **104**, 025504 (2010).
[39] C. Sanchez-Valle and J. D. Bass, Elasticity and pressure-induced structural changes in vitreous $MgSiO_3$-Enstatite to lower mantle pressures, Earth Planet. Sci. Lett. **295**, 523 (2010).
[40] S. Petitgirard, C. J. Sahle, C. Weis, K. Gilmore, G. Spiekermann, J. S. Tse, M. Wilke, C. Cavallari, V. Cerantola, and C. Sternemann, Magma properties at deep Earth's conditions from electronic structure of silica, Geochem. Persp. Lett. **9**, 32 (2019).
[41] C. J. Sahle, A. D. Rosa, M. Rossi, V. Cerantola, G. Spiekermann, S. Petitgirard, J. Jacobs, S. Huatori, M. Moretti, and A. Mirone, Direct tomography imaging for inelastic X-ray scattering experiments at high pressure, J. Synchrotron Radiat. **24**, 269 (2016).
[42] C. Sternemann and M. Wilke, Spectroscopy of low and intermediate Z elements at extreme conditions: In Situ studies of Earth materials at pressure and temperature via x-ray Raman scattering, High Press. Res. **36**, 275 (2016).
[43] M. Cotte, E. Pouyet, M. Salomé, C. Rivard, W. De Nolf, H. Castillo-Michel, T. Fabris, L. Monico, K. Janssens, T. Wang, P. Sciau, L. Verger, L. Cormier, O. Dargaud, E. Brun, D. Bugnazet, B. Fayard, B. Hesse, A. E. Pradas del Real, G. Veronesi, J. Langlois, N. Balcar, Y. Vandenberghe, V. A. Solé, J. Kieffer, R. Barrett, C. Cohen, C. Cornu, R. Baker, E. Gagliardini, E. Papillon, and J. Susini, The ID21 X-ray and infrared microscopy beamline at the ESRF: Status and recent applications to artistic materials, J. Anal. At. Spectrom. **32**, 477 (2017).
[44] G. Shen, Y. Wang, A. Dewaele, C. Wu, D. E. Fratanduono, J. Eggert, S. Klotz, K. F. Dziubek, P. Loubeyre, O. Fat'yanov V, P. D. Asimow, T. Mashimo, R. M. M. Wentzcovitch, J. Bass, Y. Bi, D. He, K. Khishchenko V, K. Leinenweber, B. Li, T. Sakai, T. Tsuchiya, K. Shimizu, D. Yamazaki, M. Mezouar, and I. T. Grp, Toward an international practical pressure scale: A proposal for an IPPS Ruby gauge (IPPS-Ruby2020), High Press. Res. **40**, 299 (2020).
[45] Y. Akahama and H. Kawamura, Pressure calibration of diamond anvil Raman gauge to 310 GPa, J. Appl. Phys. **100**, 043516 (2006).

[46] S. Petitgirard, W. J. Malfait, B. Journaux, I. E. Collings, E. S. Jennings, I. Blanchard, I. Kantor, A. Kurnosov, M. Cotte, T. Dane, M. Burghammer, and D. C. Rubie, SiO_2 Glass Density to Lower-Mantle Pressures, Phys. Rev. Lett. **119**, 215701 (2017).

[47] S. Petitgirard, G. Spiekermann, K. Glazyrin, J. Garrevoet, and M. Murakami, Density of amorphous GeO_2 to 133 GPa reveals a pyrite-like structure and stiffness at high-pressure, Phys. Rev. B **100**, 214104 (2019).

[48] S. Petitgirard, Density and structural changes of silicate glasses under high pressure, High Press. Res. **37**, 200 (2017).

[49] L. Levien, C. T. Prewitt, and D. J. Weidner, Structure and elastic properties of quartz at pressure, Am. Miner. **65**, 920 (1980).

[50] I. Kantor, V. Prakapenka, A. Kantor, P. Dera, A. Kurnosov, S. Sinogeikin, N. Dubrovinskaia, and L. Dubrovinsky, BX90: A new diamond anvil cell design for x-ray diffraction and optical measurements, Rev. Sci. Instrum. **83**, 125102 (2012).

[51] T. Kimura and M. Murakami, Fluid-like elastic response of superionic NH3 in Uranus and Neptune, Proc. Natl. Acad. Sci. USA **118**, e2021810118 (2021).

[52] M. Murakami, Silicate Glasses under Ultrahigh Pressure Conditions, in *Magmas under Pressure: Advances in High-Pressure Experiments on Structure and Properties of Melts*, edited by Y. Kono and C. Sanloup (Elsevier, 2018), pp. 371–386.

[53] C. H. Whitfield, E. M. Brody, and W. A. Bassett, Elastic moduli of NaCl by Brillouin scattering at high-pressure in a diamond anvil cell, Rev. Sci. Instrum. **47**, 942 (1976).

[54] S. Huotari, C. J. Sahle, C. Henriquet, A. Al-Zein, K. Martel, L. Simonelli, R. Verbeni, H. Gonzalez, M.-C. Lagier, C. Ponchut, M. M. Sala, M. Krisch, and G. Monaco, A large-solid-angle X-ray Raman scattering spectrometer at ID20 of the European Synchrotron Radiation Facility, J. Synch. Radiat. **24**, 521 (2017).

[55] S. Petitgirard, J. Jacobs, V. Cerantola, I. E. Collings, R. Tucoulou, L. Dubrovinsky, and C. J. Sahle, A versatile diamond anvil cell for x-ray inelastic, diffraction and imaging studies at synchrotron facilities, Rev. Sci. Instrum. **90**, 095107 (2019).

[56] C. J. Sahle, A. Mirone, J. Niskanen, J. Inkinen, M. Krisch, and S. Huotari, Planning, performing and analyzing x-ray raman scattering experiments, J. Synchrotron Radiat. **22**, 400 (2015).

[57] K. S. Scheidl, A. Kurnosov, D. M. Trots, T. B. Ballaran, R. J. Angel, and R. Miletich, Extending the single-crystal quartz pressure gauge up to hydrostatic pressure of 19 GPa, J. Appl. Crystallogr. **49**, 2129 (2016).

[58] D. Andrault, R. J. Angel, J. L. Mosenfelder, and T. Le Bihan, Equation of state of stishovite to lower mantle pressures, Am. Miner. **88**, 301 (2003).

[59] J. S. Tse and D. D. Klug, Mechanical Instability of Alpha-Quartz - A Molecular Dynamics Study, Phys. Rev. Lett. **67**, 3559 (1991).

[60] P. Gillet, Raman spectroscopy at high pressure and high temperature. Phase transitions and thermodynamic properties of minerals, Phys. Chem. Miner. **23**, 263 (1996).

[61] M. Wu, Y. Liang, J.-Z. Jiang, and J. S. Tse, Structure and properties of dense silica glass, Sci. Rep. **2**, 398 (2012).

[62] K. J. Kingma, H. K. Mao, and R. J. Hemley, Synchrotron X-ray diffraction of SiO_2 to multimegabar pressures, High Press. Res. **14**, 363 (1996).

[63] J. S. Tse, D. D. Klug, and Y. Le Page, High-pressure densification of amorphous silica, Phys. Rev. B **46**, 5933 (1992).

[64] C. Prescher, V. B. Prakapenka, J. Stefanski, S. Jahn, L. B. Skinner, and Y. Wang, Beyond sixfold coordinated Si in SiO_2 Glass at ultrahigh pressures, Proc. Natl. Acad. Sci. USA **114**, 10041 (2017).

[65] J. Badro, P. Gillet, and J. L. Barrat, Melting and pressure-induced amorphization of quartz, Europhys. Lett. **42**, 643 (1998).

[66] Y. Shu, Y. Kono, I. Ohira, Q. Li, H. Rostislav, P. Changyong, C. Kenney-Benson, Y. Wang, and G. Shen, Observation of 9-Fold coordinated amorphous TiO_2 at high pressure, J. Phys. Chem. Lett. **11**, 374 (2020).

[67] S. J. Tracy, S. J. Turneaure, and T. S. Duffy, In Situ X-Ray Diffraction of Shock-Compressed Fused Silica, Phys. Rev. Lett. **120**, 135702 (2018).